Journal of ELECTRONIC MATERIALS, Vol. 43, No. 12, 2014
DOI: 10.1007/s11664-014-3469-7

Temperature-Dependent Giant Magnetoimpedance Effect in Amorphous Soft Magnets

M. KURNIAWAN,[1,4] R.K. ROY,[2] A.K. PANDA,[2] D.W. GREVE,[1] P. OHODNICKI,[1,3] and M.E. MCHENRY[1]

1.—Carnegie Mellon University, Pittsburgh, PA, USA. 2.—CSIR National Metallurgical Laboratory, Jamshedpur, India. 3.—National Energy Technology Laboratory, Pittsburgh, PA, USA. 4.—e-mail: mkurniaw@andrew.cmu.edu

Giant magnetoimpedance (GMI)-based devices offer potential as next-generation low-cost, flexible, ultrasensitive sensors. They can be used in applications that include current sensors, field sensors, stress sensors, and others. Challenging applications involve operation at high temperatures, and therefore studies of GMI temperature dependence and performance of soft magnetic materials are needed. We present a high-temperature GMI study on an amorphous soft magnetic microwire from room temperature to 560°C. The GMI ratio was observed to be nearly constant at ~86% at low temperatures and to decrease rapidly at ~290°C, finally reaching a near-zero value at 500°C. The rapid drop in GMI ratio at 290°C is associated with a reduction in the long-range ferromagnetic order as measured by the spontaneous magnetization (M) at the Curie temperature (T_c). We also correlated the impedance with the magnetic properties of the material. From room temperature to 290°C, the impedance was found to be proportional to the square root of the magnetization to magnetic anisotropy ratio. Lastly, $M(T)$ has been fit using a Handrich–Kobe model, which describes the system with a modified Brillouin function and an asymmetrical distribution of exchange interactions. We infer that the structural fluctuations of the amorphous phase result in a relatively small asymmetry in the fluctuation parameters.

Key words: Soft magnets, high temperature, giant magnetoimpedance, permeability, skin effect, amorphous

INTRODUCTION

Amorphous and nanocrystalline soft magnetic materials exhibit properties that render them suitable for applications such as power transformers, motors, electromagnetic shielding, and sensing devices.[1,2] In the sensors arena, there has been growing interest in GMI-based sensing devices due to their low cost, flexibility, and superior sensitivity compared with current technologies.[3,4] While giant magnetoresistance (GMR)-based sensors have typical field sensitivity of ~1%/Oe, the sensitivity of GMI-based sensors can be as high as ~500%/Oe.[3] For magnetic field sensing applications at high temperatures, such as directional drilling in oil and gas extraction, soft magnetic materials with good high-temperature performance are necessary.[5] The interplay between the long-range ferromagnetic order, the magnetic anisotropy, and the measured GMI response as a function of temperature is also very interesting from a fundamental point of view. Thus, there is a need to study the temperature dependence of the GMI performance of soft magnetic materials.

GMI is a phenomenon in which the electrical impedance of a conductor under an alternating-current (AC) field changes in the presence of a direct-current (DC) magnetic field. As a function of the external DC magnetic field (H), the GMI ratio is expressed as

$$\mathrm{GMI}(\%) = \frac{\Delta Z}{Z} \times 100\% = \frac{Z(H) - Z(H_o)}{Z(H_o)} \times 100\%, \quad (1)$$

(Received August 12, 2014; accepted October 8, 2014; published online October 25, 2014)

where H_o is the DC magnetic field that results in saturation of the electrical impedance.[3,4] In the frequency range of ~100 kHz to a few MHz, the origin of the GMI effect is related to the skin effect, characterized by a skin depth δ_m given by

$$\delta_m = \frac{c}{\sqrt{4\pi^2 f \sigma \mu_\phi}}, \quad (2)$$

where c is the speed of light, f is the frequency of the AC field, σ is the conductivity, and μ_ϕ is the magnetic permeability.[3] As a function of DC magnetic field, the change in the magnetic permeability and the skin depth will result in the GMI effect. From the simple expression above, one can deduce that building sensors with large GMI ratio will require soft magnets with high transverse (ribbon) or circumferential (wire) magnetic permeability.

Studies on the temperature dependence of GMI invoke discussions of the exchange interaction and the magnetic anisotropy of the system. Previous works on the temperature effect on GMI have mostly considered the range below room temperature, where the lower GMI ratio is correlated with a reduction in magnetic permeability due to the stronger exchange interactions and larger magnetic anisotropy.[6–9] Above room temperature and below the Curie temperature T_c^{am}, thermal fluctuation weakens the exchange interactions and relieves structural stress, resulting in temperature dependence of the magnetic permeability of the material.[10,11]

Using the Handrich–Kobe model[12,13] with the modified Brillouin function developed by Gallagher et al., the magnetization curve as a function of temperature, $M(T)$, can be fit using an asymmetrical distribution of the exchange interactions.[14] The asymmetry was proposed based on knowledge of the Bethe–Slater curve, and better fitting to the $M(T)$ curve was obtained by using two distribution parameters. Based on the fitting result, these two distribution parameters can provide insight into the structural fluctuations and their consequent influence on exchange interactions in an amorphous alloy system.[15]

EXPERIMENTAL PROCEDURES

The amorphous microwire with composition $(Co_{94}Fe_6)_{72.75}Si_{12.25}B_{13.25}Cr_{1.75}$ studied in this work was prepared using the in-rotating-water quenching technique. The details of the processing technique have been described in prior work.[16–18] The diameter of the microwire was measured to be 80 μm. Our high-temperature GMI setup consists of a Thermolyne 21100 tube furnace, an Agilent 4285A impedance analyzer, and a Hewlett Packard 6031A DC power supply and solenoid with 16 turns/cm, capable of generating DC magnetic fields up to 220 Oe. The frequency of the AC field in our measurements was set to 2 MHz, where we found our GMI ratio to be highest. For our high-temperature GMI measurements, 15 cm of microwire was connected to the impedance analyzer in the four-point probe arrangement. Data acquisition was performed for decreasing temperature from 560°C to 20°C at intervals of 30°C. Curves of GMI versus T and Z_{mag} versus T were obtained by plotting the GMI ratio and the magnetic component of the impedance, both at zero applied field (H = 0 Oe), respectively, as functions of temperature. Z_{mag} here is defined as the difference between the measured electrical impedance and the impedance at the saturation state. The magnetization versus temperature curve was obtained using a Quantum Design physical property measurement system (PPMS).

RESULTS AND DISCUSSION

At room temperature (20°C), the GMI ratio of $(Co_{94}Fe_6)_{72.75}Si_{12.25}B_{13.25}Cr_{1.75}$ amorphous microwire was found to be 86.8% (Fig. 1a). This value showed very small variation (±2%) up to 260°C. Above 260°C, the GMI ratio started to decrease, and the drop became more substantial in the 290°C to 320°C temperature range. In this temperature range, the GMI ratio was also observed to be very sensitive to slight temperature fluctuations, as shown by the error bar at 290°C. Finally, above 500°C, the GMI ratio reached a near-zero value. The data suggest the presence of a "GMI tail" at 320°C to 500°C similar to the Curie tail that has been observed in magnetization versus temperature curves.[15,19,20] This observation, along with the large spread of data points at 290°C, indicates that the GMI measurement is very sensitive to minute changes in the magnetic state of the material.[3,4] GMI versus applied field curves at a few selected temperatures are shown in Fig. 1b. The peaks of these curves lie below 0.5 Oe, and are shown in the inset.

The rapid decrease in the GMI ratio at ~290°C (Fig. 1a) correlates well with the collapse of the magnetization at the Curie temperature of the amorphous phase T_c^{am} at ~282°C (Fig. 2). A work by Chiriac et al. also found that the GMI ratio of $Co_{68.15}Fe_{4.35}Si_{12.5}B_{15}$ amorphous microwire decreases to a near-zero value above T_c^{am}.[11] Chen et al. reported a similar observation in a high-temperature GMI study on nanocrystalline $Fe_{73.0}Cu_{1.0}Nb_{2.5}V_{1.0}Si_{13.5}B_{9.0}$ ribbon.[10] In their work, however, a GMI peak was observed at a temperature near T_c^{am}. At temperatures higher than T_c^{am}, the ferromagnetic to paramagnetic transition of the amorphous phase results in uncoupling of the magnetization of the crystalline phase. From both a scientific and engineering point of view, this is a very important finding. Since the Curie temperature of the amorphous phase (T_c^{am}) is typically lower than that of the crystalline phase (T_c^{xtal}), T_c^{am} would practically be the upper temperature limit above which GMI devices will fail to operate.

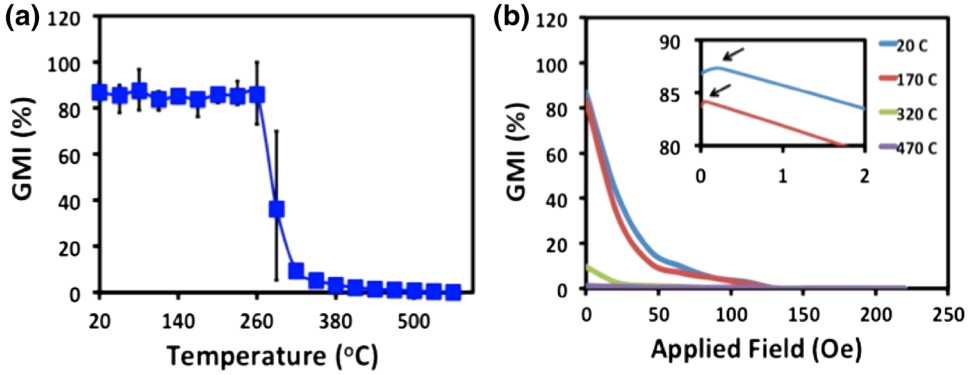

Fig. 1. (a) GMI versus temperature curve of $(Co_{94}Fe_6)_{72.75}Si_{12.25}B_{13.25}Cr_{1.75}$ amorphous microwire. The GMI ratio was observed to be constant from room temperature up to ~260°C. A rapid drop in GMI ratio occurs at ~290°C, and a near-zero value (0.72%) at saturation is reached at 500°C. The error bars denote the distribution of data points from five independent measurements. (b) GMI versus applied field curves at a few selected temperatures. The inset shows the magnified GMI versus applied field curves, exhibiting peaks at very small applied field (<0.5 Oe).

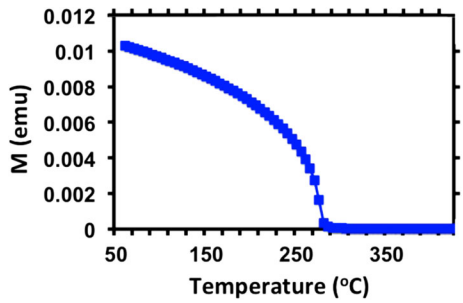

Fig. 2. Magnetization versus temperature curve of $(Co_{94}Fe_6)_{72.75}Si_{12.25}B_{13.25}Cr_{1.75}$ amorphous microwire. The Curie temperature of the amorphous phase T_c^{am} was found to be ~282°C. Applied field of 100 Oe was used during the measurements.

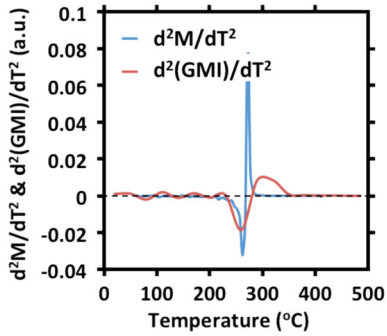

Fig. 3. Second derivative of M versus T curve and GMI versus T curve. The zero crossing for M versus T and GMI versus T lies at 272°C and 277°C, respectively (plotted in arbitrary units).

Figure 3 shows a quantitative comparison between the profile of M versus T and GMI versus T curves. Here, we approximate T_c^{am} by using the inflection point (T_{inf}), i.e., the temperature at which the gradient of the curve changes sign.[21,22] By taking the second derivative of both curves, we obtained 272°C and 277°C as T_{inf} for the M versus T and GMI versus T curve, respectively. Two observable peaks for each curve can also be used to determine the temperature range where the magnetization and GMI decrease most rapidly, i.e., 262°C to 272°C and 260°C to 300°C, respectively. The second-derivative curve of the M versus T curve exhibits a much sharper feature than that of the GMI versus T curve, due in part to the relatively larger temperature step used during the measurement of the latter (ΔT = 30°C).

Previous works have studied the relationship between the impedance and the magnetic permeability.[6,11] One can go further and correlate the impedance with the magnetization and the magnetic anisotropy of the material as follows:

$$Z_{mag}(T) \propto \frac{1}{\delta_m(T)} \propto \mu_\phi(T)^{1/2} \propto \left(\frac{M_s(T)}{H_k(T)}\right)^{1/2} \quad (3)$$

The magnetic anisotropy of a material can be extracted from its GMI profile. By plotting the applied field that results in the maximum GMI value (Fig. 1b) as a function of temperature, the magnetic anisotropy (H_k versus T) curve was estimated based upon arguments presented in prior published works (Fig. 4).[10,23] At the anisotropy field, the magnetic permeability changes most abruptly due to the switching of the magnetization dynamics from domain wall motion to magnetization rotation.[24,25] Figure 4 shows a decreasing magnetic anisotropy with increasing temperature in the 20°C to 290°C range. Close to T_c^{am} (290°C), the magnetic anisotropy drops rapidly and becomes unobservable at higher temperature.

Chiriac et al. directly measured the temperature-dependent circumferential permeability and correlated it with the observed GMI.[11] In this work, we obtained the temperature-dependent magnetic anisotropy (μ_ϕ versus T) indirectly by taking the ratio of the magnetization (M versus T) to the magnetic anisotropy (H_k versus T). This step implicitly assumes: (1) the magnetization curve obtained with DC magnetic field (static mode) and AC magnetic field (dynamic mode) exhibit the same

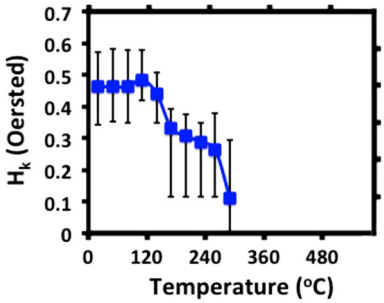

Fig. 4. Magnetic anisotropy (H_k) plotted as a function of temperature. Above T_c^{am} (290°C), the magnetic anisotropy was unobservable.

temperature dependence, and (2) the anisotropy field along the longitudinal axis has the same temperature dependence as the anisotropy field along the circumferential direction. Figure 5 shows the magnetic component of the impedance and the square root of the magnetization to magnetic anisotropy ratio as functions of temperature with arbitrary units. Their similar temperature dependence agrees with the expression in Eq. 3. From room temperature to 260°C, a small variation in the impedance and the magnetization to magnetic anisotropy ratio were observed. At T_c^{am} (290°C), both curves drop rapidly, consistent with the postulate that the magnetic coupling collapses at this temperature and thus results in a large decrease of the magnetic permeability.[10,11]

The typical T_c^{am} values of amorphous Fe-rich and Co-rich alloys are in the 200°C to 400°C range, though higher T_c values are observed in closer to equiatomic materials.[27,28] Based on the Bethe–Slater curve, the highest T_c^{am} in the Fe-Co system lies in the Co-rich side. The fact that the T_c^{am} of the amorphous alloy studied in this work (~290°C) is much lower than the T_c^{am} of pure Fe (767°C) or pure Co (1127°C) is due to the reduction in the number of exchange bonds between Fe-Fe, Co-Co, and Fe-Co which results from alloying these elements with the glass formers (e.g., Nb, B).[26] In essence, the T_c^{am} of an amorphous alloy is dependent on key factors such as the number, type, and strength of exchange bonds between the constituents.

To study the distribution of the exchange interactions in our $(Co_{94}Fe_6)_{72.75}Si_{12.25}B_{13.25}Cr_{1.75}$ amorphous microwire, we used the Handrich–Kobe model with a modified Brillouin function to fit the M versus T curve. In the original version of the theory, Handrich and Kobe proposed an expression that describes the magnetization as a function of temperature as[12,13]

$$\sigma(T) = \frac{1}{2}\{B_s([1+\delta]x) + B_s([1-\delta]x)\}, \qquad (4)$$

where

$$x = \frac{3S}{S+1}\frac{\sigma}{t} \quad \text{and} \quad t = \frac{T}{T_c}, \qquad (5)$$

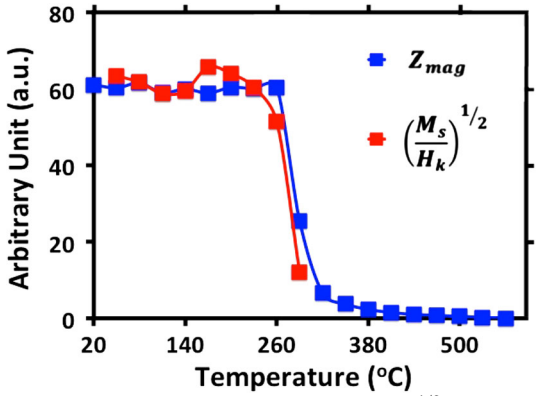

Fig. 5. Comparison of Z_{mag} versus T and $\left(\frac{M_s}{H_k}\right)^{1/2}$ versus T with arbitrary units. The $\left(\frac{M_s}{H_k}\right)^{1/2}$ curve shown here is from room temperature to T_c^{am} (290°C).

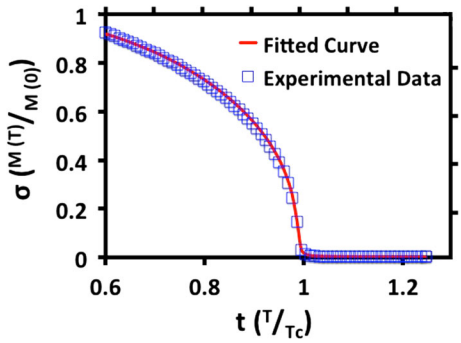

Fig. 6. Handrich–Kobe model with modified Brillouin function using asymmetrical distribution of exchange interactions to fit the $M(T)$ curve. The best fit was obtained for $\delta_+ = 0.012$ and $\delta_- = 0.05$.

with $\sigma(T)$ being the reduced magnetization, defined as $\sigma(T) = M(T)/M(0)$. The fluctuation parameter δ is related to the exchange interaction fluctuation ΔJ by $\delta = (\langle \Delta J \rangle^2 / \langle J \rangle^2)^{0.5}$. However, a better fit to our M versus T curve was obtained using two fluctuation parameters, δ_+ and δ_-, resulting in an asymmetrical distribution of exchange interactions (Fig. 6). As developed by Gallagher et al., the modified Handrich–Kobe model is now[14,15]:

$$\sigma(T) = \frac{1}{2}\{B_s([1+\delta_+]x) + B_s([1-\delta_-]x)\}. \qquad (6)$$

The Bethe–Slater curve explains the dependence of the exchange interaction on the interatomic spacing. For systems in the amorphous state, the fluctuation in interatomic spacing can result in an asymmetric distribution of exchange interaction.[14] The best fit to our M versus T curve was obtained with $\delta_+ = 0.012$ and $\delta_- = 0.05$. These fluctuation parameters show relatively small asymmetry in the distribution of exchange interactions compared with previous studies.[14,15] This result corresponds well with the insensitivity of Co-Fe alloys (relative to

Fe-rich alloys) to fluctuation, since these systems lie nearer the peak in the Bethe–Slater curve.[14]

GMI has also been studied in nanocomposite alloys.[29–31] The temperature dependence of the GMI in Co-based nanocomposite alloys will be more complicated as: (1) the exchange coupling[32] between the amorphous and nanocrystalline phases and the T dependence of the induced anisotropies must be considered;[33,34] (2) multiple crystalline phases are observed to form, some of which are highly faulted;[32,35–37] and (3) relatively large induced anisotropies are obtainable through magnetic field or strain annealing.[34,38] This richer T dependence will be explored further in future publications.

CONCLUSIONS

The temperature dependence of the GMI performance of a $(Co_{94}Fe_6)_{72.75}Si_{12.25}B_{13.25}Cr_{1.75}$ amorphous microwire is presented. The rapid decrease of the GMI ratio is correlated with the collapse of the magnetization of the amorphous phase at T_c^{am}. This finding is of special importance since T_c^{am} is found to be the upper limit for operation of GMI devices. Future works on soft magnetic materials with improved T_c^{am} will open doors to utilization of GMI-based sensing devices in extreme temperature environments. From the theoretical point of view, we correlated the impedance with the magnetization and the magnetic anisotropy of the material. Our finding shows that the impedance is proportional to the square root of the magnetization to magnetic anisotropy ratio from room temperature to T_c^{am}. Using the modified Handrich–Kobe model to fit our magnetization data, we found low asymmetry in the distribution of the exchange interactions in our system. This finding agrees with the stability of Co-Fe alloys with respect to structural fluctuation based on knowledge of the Bethe–Slater curve.

ACKNOWLEDGEMENTS

M.E.M. and M.K. acknowledge support from the Army Research Laboratory (Contract No. DEAR-0000219). M.E.M. acknowledges support from the Research for Advanced Manufacturing in Pennsylvania program (Contract No. C000052427). D.W.G. acknowledges support from NETL (Contract No. RES1000025/169). This report was prepared as an account of work sponsored by an agency of the United States Government. Neither the United States Government nor any agency thereof, nor any of their employees, makes any warranty, express or implied, or assumes any legal liability or responsibility for the accuracy, completeness, or usefulness of any information, apparatus, product, or process disclosed, or represents that its use would not infringe privately owned rights. Reference herein to any specific commercial product, process, or service by trade name, trademark, manufacturer, or otherwise does not necessarily constitute or imply its endorsement, recommendation, or favoring by the United States Government or any agency thereof. The views and opinions of authors expressed herein do not necessarily state or reflect those of the United States Government or any agency thereof.

REFERENCES

1. M.E. McHenry, M.A. Willard, and D.E. Laughlin, *Prog. Mater. Sci.* 44, 291 (1999). doi:10.1016/S0079-6425(99)00002-X.
2. A.M. Leary, P.R. Ohodnicki, and M.E. McHenry, *JOM* (2012). doi:10.1007/s11837-012-0350-0.
3. M.H. Phan and H.X. Peng, *Prog. Mater. Sci.* 53, 323 (2008). doi:10.1016/j.pmatsci.2007.05.003.
4. C. Tannous and J. Gieraltowski, *J. Mater. Sci.* 15, 125 (2004). doi:10.1023/B:JMSE.0000011350.93694.91.
5. J.T. Finger, A.J. Mansure, S.D. Knudsen, and R.D. Jacobson, *Soc. Petrol. Eng.* (2003). doi:10.2118/79884-MS.
6. M.H. Phan, H.X. Peng, M.R. Wisnom, S.C. Yu, and N. Chau, *Phys. Status Solidi* 201, 1558 (2004). doi:10.1002/pssa.200306791.
7. Y.K. Kim, W.S. Cho, T.K. Kim, C.O. Kim, and H. Lee, *J. Appl. Phys.* 83, 6575 (1998). doi:10.1063/1.367605.
8. M.M. Tehranchi, M. Ghanaatshoar, S.M. Mohseni, M. Coisson, and M. Vazquez, *J. Non-Cryst. Solids* 351, 2983 (2005). doi:10.1016/j.jnoncrysol.2005.06.049.
9. P. Marin, M. Vazquez, J. Arcas, and A. Hernando, *J. Magn. Magn. Mater.* 203, 6 (1999). doi:10.1016/S0304-8853(99)00173-0.
10. G. Chen, X.L. Yang, L. Zeng, J.X. Yang, F.F. Gong, D.P. Yang, and Z.C. Wang, *J. Appl. Phys.* 87, 5263 (2000). doi:10.1063/1.373315.
11. H. Chiriac, C.S. Marinescu, and T.A. Ovari, *J. Magn. Magn. Mater.* 196, 162 (1999). doi:10.1016/S0304-8853(98)00702-1.
12. K. Handrich, *Phys. Status Solidi* 32, K55 (1969). doi:10.1002/pssb.19690320166.
13. S. Kobe, *Phys. Status Solidi* 41, K13 (1970). doi:10.1002/pssb.19700410153.
14. K.A. Gallagher, M.A. Willard, V.N. Zabenkin, D.E. Laughlin, and M.E. McHenry, *J. Appl. Phys.* 85, 8 (1999). doi:10.1063/1.369100.
15. N.J. Jones, H. Ucar, J.J. Ipus, M.E. McHenry, and D.E. Laughlin, *J. Appl. Phys.* 111, 07A334 (2012). doi:10.1063/1.3679456.
16. P. Sarkar, R.K. Roy, A.K. Panda, and A. Mitra, *Appl. Phys. A* 111, 575 (2013). doi:10.1007/s00339-012-7260-4.
17. P. Sarkar, R.K. Roy, A. Mitra, A.K. Panda, M. Churyukanova, and S. Kaloshkin, *J. Magn. Magn. Mater.* 324, 2543 (2012). doi:10.1016/j.jmmm.2012.03.041.
18. L.V. Panina and K. Mohri, *Appl. Phys. Lett.* 65, 1189 (1994). doi:10.1063/1.112104.
19. H. Ucar, J.J. Ipus, V. Franco, M.E. McHenry, and D.E. Laughlin, *JOM* (2012). doi:10.1007/s11837-012-0349-6.
20. J.J. Ipus, H. Ucar, and M.E. McHenry, *IEEE Trans. Magn.* 47, 10 (2011). doi:10.1109/TMAG.2011.2159781.
21. K. Fabian, V.P. Shcherbakov, and S.A. McEnroe, *Geochem. Geophys. Geosyst.* 14, 4 (2013). doi:10.1029/2012GC004440.
22. R.L. Hadimani, Y. Melikhov, J.E. Snyder, and D.C. Jiles, *J. Magn. Magn. Mater.* 320, e696 (2008). doi:10.1016/j.jmmm.2008.04.035.
23. L.V. Panina, K. Mohri, T. Uchiyama, and M. Noda, *IEEE Trans. Magn.* 31, 1249 (1995). doi:10.1109/20.364815.
24. H. Chiriac and T.A. Ovari, *Prog. Mater. Sci.* 40, 333 (1996). doi:10.1016/S0079-6425(97)00001-7.
25. M.H. Phan, H.X. Peng, M.R. Wisnom, and S.C. Yu, *J. Appl. Phys.* 98, 014316 (2005). doi:10.1063/1.1953864.
26. R.C. O'Handley, *J. Appl. Phys.* 62, R15 (1987). doi:10.1063/1.339065.
27. S.J. Kernion, K.J. Miller, S. Shen, V. Keylin, J. Huth, and M.E. McHenry, *IEEE Trans. Magn.* 47, 3452 (2011). doi:10.1109/TMAG.2011.2157326.
28. K.J. Miller, A. Wise, A. Leary, D.E. Laughlin, V. Keylin, J. Huth, and M.E. McHenry, *J. Appl. Phys.* 107, 09A316 (2010). doi:10.1063/1.3350900.

29. S. Dwevedi, G. Markandeyulu, P.R. Ohodnicki, A. Leary, and M.E. McHenry, *J. Magn. Magn. Mater.* 323, 1929 (2011). doi:10.1016/j.jmmm.2011.02.006.
30. N. Laurita, A. Chaturvedi, C. Bauer, P. Jayathilaka, A. Leary, C. Miller, M.H. Phan, M.E. McHenry, and H. Srikanth, *J. Appl. Phys.* 109, 07C706 (2011). doi:10.1063/1.3548857.
31. A. Chaturvedi, N. Laurita, A. Leary, M.H. Phan, M.E. McHenry, and H. Srikanth, *J. Appl. Phys.* 109, 07B508 (2011). doi:10.1063/1.3540403.
32. P.R. Ohodnicki, V. Keylin, H.K. McWilliams, D.E. Laughlin, and M.E. McHenry, *J. Appl. Phys.* 103, 07E740 (2008). doi:10.1063/1.2839284.
33. P.R. Ohodnicki, D.E. Laughlin, M.E. McHenry, V. Keylin, and J. Huth, *J. Appl. Phys.* 105, 07A32224 (2009). doi:10.1063/1.3068547.
34. P.R. Ohodnicki, J. Long, D.E. Laughlin, M.E. McHenry, V. Keylin, and J. Huth, *J. Appl. Phys.* 104, 113909 (2008). doi:10.1063/1.3021141.
35. P.R. Ohodnicki, Y.L. Qin, D.E. Laughlin, M.E. McHenry, M. Kodzuka, T. Ohkubo, K. Hono, and M.A. Willard, *Acta Mater.* 57, 87 (2009). doi:10.1016/j.actamat.2008.08.051.
36. P.R. Ohodnicki, D.E. Laughlin, M.E. McHenry, and M. Widom, *Acta Mater.* 58, 4804 (2010). doi:10.1016/j.actamat.2010.05.015.
37. P.R. Ohodnicki, Y.L. Qin, M.E. McHenry, D.E. Laughlin, and V. Keylin, *J. Magn. Magn. Mater.* 322, 315 (2010). doi:10.1016/j.jmmm.2009.09.047.
38. S.J. Kernion, P.R. Ohodnicki, J. Grossman, A. Leary, S. Shen, V. Keylin, J. Huth, J. Horwath, M.S. Lucas, and M.E. McHenry, *Appl. Phys. Lett.* 101, 102408 (2012). doi:10.1063/1.4751253.